Journal of
Materials Chemistry B

ROYAL SOCIETY OF CHEMISTRY

PAPER

View Article Online
View Journal | View Issue

Check for updates

Cite this: J. Mater. Chem. B, 2017, 5, 3580

Highly selective organic transistor biosensor with inkjet printed graphene oxide support system†

Dong-Hoon Lee,[a] Hee-Sang Cho,[b] Dawoon Han,[a] Rohit Chand,[a] Tae-Jong Yoon*[b] and Yong-Sang Kim *[a]

Received 26th December 2016, Accepted 27th March 2017

DOI: 10.1039/c6tb03357a

rsc.li/materials-b

Most of the reported field effect transistors (FETs) fall short of a general method to uniquely specify and detect a target analyte. For this reason, we propose a pentacene-based FET with a graphene oxide support system (GOSS), composed of functionalized graphene oxide (GO) ink. The GOSS with a specific moiety group to capture the biomaterial of interest was inkjet printed on the pentacene FET. It provided modular receptor sites on the surface of pentacene, without alteration of the device. To evaluate the performance of a GOSS-pentacene FET biosensor, we detected the artificial DNA and circulating tumor cells as a proof-of-concept. The mobility of the FET dramatically changed upon capturing the target biomolecule on the GOSS. The FET exhibited high selectivity with 0.1 pmoles of the target DNA and a few cancer cells per detection volume. This study suggests a valuable sensor for medical diagnosis that can be mass produced effortlessly at low-cost.

1 Introduction

In the era of an aging population, detection of diseases and their prevention using diagnostic devices are becoming increasingly important.[1] The diagnostic devices need to be accurate, rapid, cost effective, and portable. Detection of cancer markers like DNA or circulating tumor cells (CTCs) in peripheral blood through biopsies is commonly applied to confirm metastatic cancer in patients.[2,3] To monitor the cancer markers in blood, the biopsy sample needs pre-treatment such as labeling or isolation because of the extremely rare population and has a complex detection sequence with long analysis time.[4–6] Accordingly, many researchers have focused on electrochemical biosensors, due to their label-free process and simple detection sequence.[7,8]

Recently, field effect transistor (FET) based biosensors have shown good prospects to be used as diagnostic devices in the healthcare system due to their tunability, small dimension, low-cost, and possibility of integrating different types of sensors on the same chip with logic circuit analysis.[9,10] The pentacene-based organic FET is a promising candidate for future biosensors due to its flexibility and biocompatibility.[11,12] However, due to the lack of tunable properties, pentacene in its natural form can only be used for the detection of DNA.[13,14] Most FET biosensors directly detect the change in the gate voltage–drain current from the electrical potential difference induced by the intrinsic charge of biomolecular interactions.[15,24] Sensing on the active layer is highly sensitive, as it dramatically alters the current value of the FET due to a change in carrier mobility.[16] Although most of the organic semiconductors are naturally sensitive to several bio-molecular interactions, they still lack the ability to detect a wide range of analytes. Functionalization of the sensing layer is a prerequisite to obtaining a selective and sensitive sensor, but it is complex due to organic material's weak chemical resistance.

Among various functionalization methods, the self-assembled monolayer (SAM) is widely used to immobilize the receptor or probes on the sensing layer.[17] Despite the reproducible property of the SAM, it is restrictive because of the dipping-process, which can damage the sensor or alter its properties.[18] Most of the functionalization processes for an organic semiconductor can result in a decrease in device performance, morphology, and loss of stability. To overcome these limitations, many researchers have inclined towards the designing of new organic semiconductors or printing of probes, instead of complex surface treatment to fabricate biosensors.[19] Screen printing, gravure printing, nano-imprinting, or inkjet printing can be used to immobilize receptors in the required area on any type of substrate. The printing of biomolecules is advantageous to realize a multiplex and array of biosensors at low-cost with commercial standards. It allows complex patterning of very small volumes of ink (picoliters) at high resolution.[18] For this reason, many groups have reported biosensors such as pH,[20] glucose,[21] C-reactive protein,[19] and DNA[22] using inkjet printing.

Graphene has also emerged as a material of interest. It has a large surface area, high electrical conductivity, excellent mechanical strength, and can be functionalized. Its outstanding properties

[a] School of Electronic and Electrical Engineering, Sungkyunkwan University, Suwon, Gyeonggi, 16419, South Korea. E-mail: yongsang@skku.edu
[b] Nano-bio Materials Chemistry Lab, College of Pharmacy, Ajou University, Suwon, Gyeonggi, 16499, South Korea

† Electronic supplementary information (ESI) available. See DOI: 10.1039/c6tb03357a

have influenced its applications in numerous fields. However, it still has many limitations to use in the industry with mass production. The graphene should be detached from the copper substrate before using it. During detaching, unfortunately, it experiences morphological defects such as dislocations, edge and edge-like defects, holes or wiggles of the plane.[23] Also, the alignment of a graphene oxide sheet on the desired area is also a challenging task. For this reason, many groups have focused on graphene oxide based biosensors. However, because biomolecules such as antibody on graphene oxide can be damaged during the reducing process, it should be subjected to further processing such as SAM treatment.

Therefore, in this work, we propose a graphene oxide support system (GOSS), composed of functionalized graphene oxide (GO) ink dissolved in deionized (DI) water and a pentacene based FET as a novel biosensor. The GOSS can be inkjet printed on the pentacene layer without any damage and it can be combined by a π–π bond. The GOSS was pretreated with probes and deposited by piezoelectric inkjet printing. The GOSS forms a sensing layer while the pentacene acts as an active layer. To prove the efficacy of the GOSS, functional groups and antibodies were conjugated onto the GO surface for the specific sensing of the target biomolecules. We evaluated this GOSS-pentacene FET based biosensor for the detection of target DNA or CTC.

2 Experimental

2.1 DNA and CTC preparation

30-mer single stranded (ss) DNA (polyA with terminal thiol and poly-T without thiol) was purchased from Bionics for use in this study. Thiolated polyA was diluted in DI water to 10 pmoles μm^{-1}, while the poly-T was diluted to concentrations from 100 to 0.1 pmoles μm^{-1}. As artificial floating CTCs, SkBr3 and MCF-7 cell lines were purchased from the American Type Culture Collection (ATCC, VA) and cultured in a mixing medium solution of 10% fetal bovine serum (GIPCO) and RPMI-1640 (GIPCO) at 5% CO_2 in a 37 °C incubator. To generate floating cells for applying to the microfluidic channel, the cultured cells were treated with trypsin–EDTA solution (Sigma-Aldrich) and then fixed with a paraformaldehyde (4%) solution after cell counting (1.0×10^5 mL^{-1}).

2.2 GOSS ink preparation

6-Arm polyethylene glycol amine (6 arm-PEG-amine, SunBio, P6AM-15) conjugated GO was obtained by first linking carboxylic acid functional groups on bare GO nanosheets (GO-COOH). For this, 5 g of sodium hydroxide (125 mmol, Sigma-Aldrich) and 5 g of chloroacetic acid (53 mmoL, Sigma-Aldrich) were dissolved in DI water (20 mL) and then sonicated for 2 hours after adding 30 mL of GO solution (2 mg mL^{-1}, NANO-GO-STM, Graphene Supermarket). The mixture was precipitated down to remove excess chemicals using centrifugation (13 000 rpm, 30 min) after adjusting to neutral pH with 1 N HCl solution. The precipitates were dispersed homogeneously in DI water and then the purification step was repeated. Dialysis of the dispersed solution was carried out (Cellulose Ester, membrane dialysis, MW: 50 000) for 3 days to remove excess salts, ions, and chemicals. To terminate the amine active groups on GO, 5 mL of GO-COOH (2 mg mL^{-1}) was first sonicated for 30 min after adding 20 μL of triethylamine to adjust the pH to 8. The mixture was then stirred at room temperature for 3 hours after adding 1 mL of 6-arm-PEG-amine and 0.15 mL of *N*-(3-dimethylaminopropyl)-*N*′-ethylcarbodiimide hydrochloride (EDC, 80 mg mL^{-1}, Sigma-Aldrich). The amine active GO nanosheets (GO–PEG-NH_2) were purified by the dialysis process to eliminate excess and unreacted chemicals. To obtain sulfhydryl active GO, 10 mL of GO–PEG-NH_2 (1 mg mL^{-1}) and 10 mg of sulfosuccinimidyl-4-[*N*-maleimidomethyl]cyclohexane-1-carboxylate (Sulfo-SMCC, 0.023 mmoL) were mixed for 3 hours at room temperature after adjusting the pH to 8 with sodium carbonate solution. The sulfhydryl activated GO was used for the anchoring of thiolated DNA and half antibody.

To anchor cancer specific antibody, human epidermal growth factor receptor 2 (HER2, herceptinTM, Roche, 5 mg) was dissolved in 2 mL of EDTA solution (10 mM) and treated with cysteamine (10 mg, Sigma-Aldrich) for 1 hour at room temperature to generate sulfhydryl (–SH) active half antibody. The half antibody was then purified on a PD-10 column (SephadexTM, G-25, GE Healthcare). The prepared half antibody solution (2 mL) and maleimide terminated GO were shaken for 6 hours in a 4 °C incubator. The solution was precipitated down to remove excess compounds (13 000 rpm, 30 min) and then finally dispersed in RPMI-1640 buffer.

2.3 Device fabrication

We fabricated the bottom gate/top contact structured pentacene FET as shown in Fig. 1A. A 75 nm thick aluminum layer was deposited using thermal evaporation through the shadow mask for the gate electrode on cleaned glass. The poly(methyl methacrylate) (PMMA) (Sigma-Aldrich, 4 wt% in toluene) was then spin-coated and cured in a conventional oven at 100 °C for 30 min. The gate contact area was manually etched using acetone. The 70 nm thick pentacene as an active layer was then patterned over the PMMA,

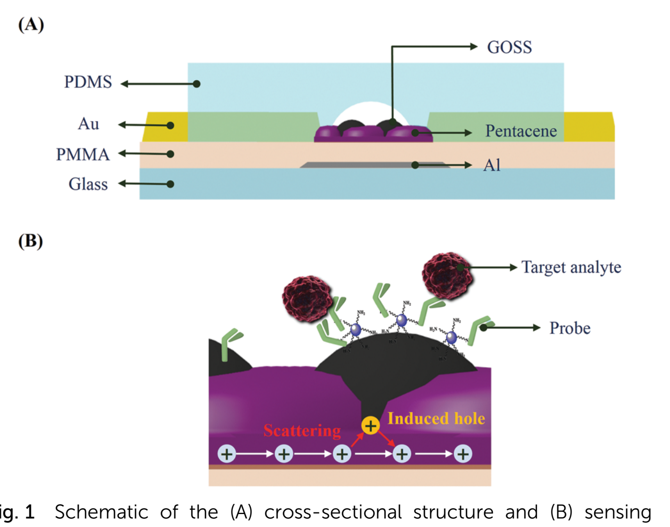

Fig. 1 Schematic of the (A) cross-sectional structure and (B) sensing mechanism of a microchannel integrated GOSS-pentacene FET biosensor.

through a shadow mask by thermal evaporation at a rate of 0.1 Å s^{-1} with the substrate temperature fixed at 85 °C. The source and drain electrodes, a 100 nm thick Au layer, were deposited through the shadow mask by thermal evaporation. The active channel of the pentacene FET was 1000 μm wide and 300 μm long. The detailed CAD design of the FET is shown in Fig. S1A (ESI†).

2.4 Evaluation of the GOSS printing technique

To deposit the GOSS layer on pentacene, we compared different printing methods such as spray coating, drop casting, fluid channel-mediated coating, and inkjet printing. The detailed comparison of all the techniques is presented in Fig. S1B (ESI†). Amongst all these methods, inkjet printing shows the best performance in terms of uniformity and reproducibility. The GO ink based GOSS was printed on the pentacene FET using an inkjet printer. The morphology of the GOSS can be controlled by altering the printing conditions, as shown in Fig. S1C (ESI†). In this study, the printing conditions were fixed with a dot to dot and line to line spacing size of 30 μm at room temperature (25 °C). Finally, a PDMS based microfluidic channel of 100 μm width was bonded on top of the FET.

2.5 DNA and CTC detection using the pentacene FET with a GOSS

For DNA sensing, 2 μL (10 pmoles μL^{-1}) of thiol functionalized ssDNA (polyA) was injected on the maleimide terminated GOSS. The thiolated DNA was allowed to bond with the maleimide group for 12 hours at 4 °C. After incubation, 2 μL of DI water was injected slowly to rinse the unbound DNA and the FET was allowed to dry for 60 min at room temperature. To carry out DNA hybridization, 2 μL (10 pmoles μL^{-1}) of complementary non-thiolated ssDNA (poly-T) was injected on the GOSS, containing immobilized polyA. The hybridization proceeded for 1 hour and then DI water was injected into the microfluidic channel for cleaning. After cleaning, the DNA immobilized pentacene FET was dried for the measurement. For CTC sensing, the HER2 conjugated GOSS was first printed on the pentacene. Next, 2 μL of CTCs associated with breast cancer was injected into the fluid channel and incubated at 35 °C for 1 hour. The concentration of CTCs was 100 cells per μL in RPMI-1640 buffer. After the reaction, RPMI-1640 buffer was then injected slowly to rinse the fluid channel and was dried for 60 min.

2.6 Characterization methods

The performance of biosensors was measured in terms of their transfer characteristic after each immobilization step, using a 4145B source measure unit. To evaluate the transfer characteristics, the $I_{DS(sat)}$ between the source and the drain as a function of V_{GS} under constant V_{DS} was measured. One of the important factors of FET is the field effect mobility of carriers in its channel region. The mobility was determined using the saturation drain current following this equation:

$$I_{DS(sat)} = \frac{WC\mu}{L}(V_{GS} - V_T)^2 \quad (1)$$

where W is the width of the channel, L is the length of the channel, C is the capacitance per unit area of the PMMA gate insulator, V_{GS} is the gate voltage and V_T is the threshold voltage. If we take the square root of eqn (1), we obtain

$$\sqrt{I_{DS(sat)}} = \sqrt{\frac{WC\mu}{L}}(V_{GS} - V_T) \quad (2)$$

As shown in the equation, the carrier mobility was proportional to the slope of the square root of $I_{DS(sat)}$. The extrapolation of the straight line to zero current gives the threshold voltage.[13]

3 Results and discussion

3.1 Characterization of the GOSS

The functionalized GO nanosheets or the GOSS were successfully prepared through simple chemical reactions (Fig. 2A). At first, the carboxylic acid functional groups on the bare GO nanosheets (GO-COOH) were generated followed by the conjugation of amine functional groups onto the GO-COOH. The amine groups were conjugated using 6-arm-PEG-amine by a simple EDC coupling method. The FT-IR study of the GOSS clearly verifies the functionalization of GO nanosheets. The various GOs in

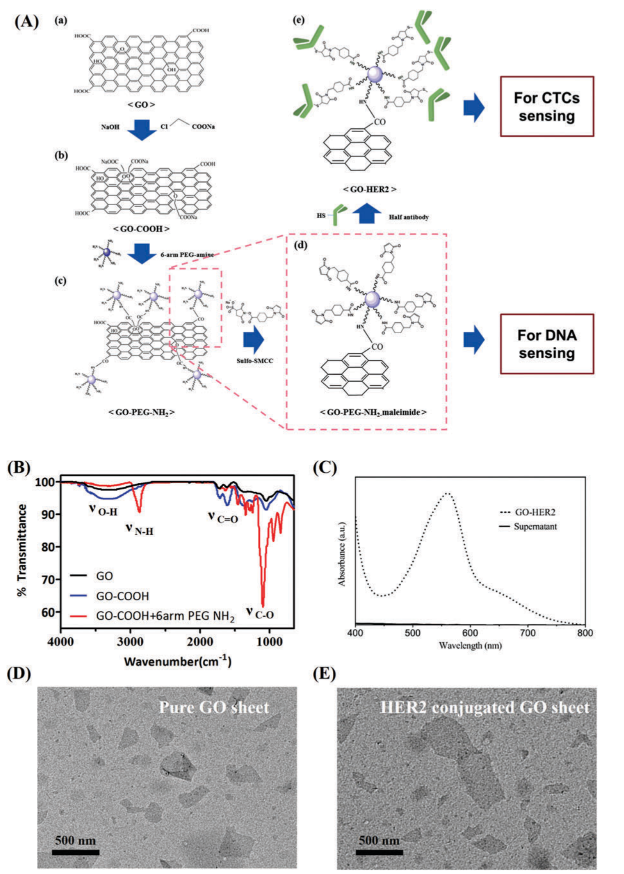

Fig. 2 Preparation of the functionalized GO ink. (A) Synthetic scheme for the fabrication of GO complexes (GO–PEG-NH_2 and GO-HER2). (B) FT-IR spectra of GO (black), GO-COOH (blue) and GO-COOH + 6 arm-PEG-NH_2 (red). (C) Absorption spectral analysis of the HER2 antibody onto the GO–PEG-NH_2. The supernatant was indicated as the only solution without the GO-HER2 composite obtained by centrifugation. TEM images of the commercial GO (D) and functionalized GO (E).

solution was characterized the charge changing by zeta potential analysis (Fig. S2, ESI†). In Fig. 2B, the blue lines show the presence of the COOH group on GO while the red line confirms the presence of the terminal amine group on GO.

The amine active GO nanosheet was then processed to create sulfhydryl groups for the immobilization of probe DNA or breast cancer-specific antibody (HER2). The amount of antibody on the GO was quantitatively analyzed with 4 nmol mg^{-1} by the BCA protein assay kit (Pierce™) (Fig. 2C). The commercial GO exhibited typical nanosheet morphology with 1–2 nm thickness in AFM as shown in Fig. S4 (ESI†). The morphology of the nanosheets and the GO-HER2 complex did not alter during the chemical reaction (Fig. 2D and E).

3.2 Characterization of the GOSS-pentacene FET

Fig. 3 shows the comparison of transfer characteristics of the pentacene FET before and after GOSS printing. The GOSS seeps into the grain boundary of pentacene and forms π–π bonding,[25] which makes a very stable sensing layer. Printing of the GOSS created a comparatively negligible change in the mobility of the FET due to a small amount of electrical potential from the GOSS as shown in Fig. S2 (ESI†) and a thick pentacene layer with a thickness of 70 nm. The minute change in the mobility is possibly due to the ions present in the GOSS and mechanical damage during printing. The inset of Fig. 3 shows the optical microscopic image of the printed GOSS on the pentacene FET. The hydrophilic GOSS self-aligned on the hydrophobic pentacene to give a mesh-like appearance. DI water was injected into the GOSS biosensor after GOSS printing to remove the non-specific GOSS on the pentacene surface. After DI water injection, we measured the SEM image of the GOSS on the pentacene surface as shown in Fig. S1D (ESI†).

3.3 Detection of DNA

The influence of DNA immobilization on the GOSS-pentacene FET was first evaluated by depositing thiolated ssDNA (polyA, 30-mer, 10 pmoles μL^{-1}). Subsequently, the complementary ssDNA (poly-T, 30-mer, 10 pmoles μL^{-1}) was injected into the fluid channel for hybridization. The hybridization of DNA strands on the GOSS and the pentacene surface was confirmed by the fluorescence imaging of FET. After the hybridization, the devices were stained with intercalating GelGreen dye and observed under a confocal microscope. The green spots in Fig. 4A and B represent the hybridized DNA (polyA + T) of FET biosensors without a GOSS and with a GOSS, respectively. The GOSS-pentacene FET captured large amounts of DNAs on the GOSS compared to the bare-pentacene FET.

The GOSS-pentacene and bare-pentacene FETs were subjected to electrical analysis before and after DNA hybridization and the difference signifies the bio-sensing of DNA. In Fig. 4C and D, the transfer characteristic based sensing performances of the pentacene FET without a GOSS and with a GOSS. The black curve represents the initial characteristic of the pentacene FET. The red and blue curves are for the immobilization of polyA and hybridization with polyT (polyA + T), respectively. As shown in the results, the mobility of the FET with a GOSS after polyA immobilization decreased from 0.097 cm^2 V^{-1} s^{-1} (initial) to 0.063 cm^2 V^{-1} s^{-1}. The hybridization of polyT further decreased the mobility to 0.044 cm^2 V^{-1} s^{-1}. On the other hand, the pentacene FET without a GOSS was less changed. The insets of Fig. 4C and D show the output characteristics at an applied gate voltage of −30 V. The output current also decreased following the decreased mobility.

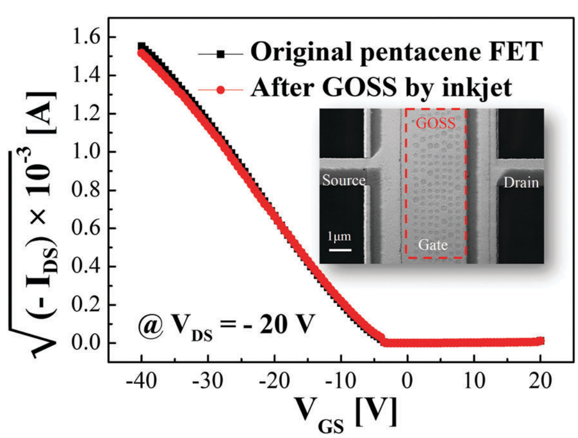

Fig. 3 The electrical properties of the pentacene FET before and after inkjet printing of GOSS on the pentacene.

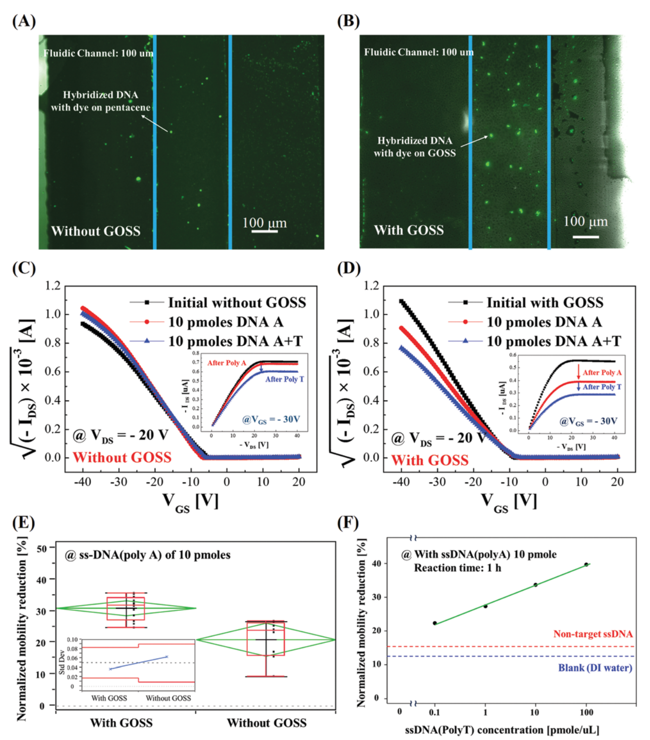

Fig. 4 Fluorescence image of the hybridized DNA (polyA + T) on (A) GOSS and (B) bare pentacene without GOSS. Electrical performance of (C) bare pentacene FET and (D) GOSS-pentacene FET. The transfer curve (V_{DS} = −20 V) of the FET before and after poly-A immobilization, and after poly-T hybridization on GOSS. (E) Change in the normalized mobility of the FET with GOSS and without GOSS after ssDNA (polyA) immobilization (n = 8). The standard deviation values of devices with GOSS and without GOSS are 0.037 and 0.063, respectively. (F) Reduction of normalized mobility of the FET depending on the poly-T concentration (0.1, 1, 10 and 100 pmoles μL^{-1}). The red line and blue line mean the change in mobility for the non-target DNA and DI water (blank), respectively.

In our previous work, the bare pentacene FET has been used to prove that the DNA can be immobilized on the pentacene surface through hydrophobic interactions.[13] However, the bare-pentacene FET does not have specific binding for biomolecules and just captures DNA by physical absorption. However, in this experiment, we make a specific binding on the pentacene surface using a GOSS which induced the enhancement of the sensing performance of the pentacene FET.

Fig. 4E shows the normalized mobility reduction of each device by the data analysis using JMP when 2 μL (10 pmoles μL^{-1}) of ssDNA (polyA) was detected. The average reduction of normalized mobility with and without the GOSS is 31% and 21%, respectively. In addition, the GOSS-pentacene FET showed much higher reproducibility, as shown in the inset of Fig. 4D. Additionally, as evident from the analysis of Fig. 4A and Fig. S3A (ESI†), a higher amount of DNA anchored to the GOSS surface than the bare pentacene surface, which shows the better sensitivity of the GOSS-pentacene biosensor. Based on these results, the pentacene FET with a GOSS has better bio-sensing ability than the bare pentacene FET.

The electrical properties of the FET dramatically changed due to the negative charge on DNA imparted by the phosphate group. The negative charge attracts holes at the grain-boundary of the pentacene layer and induces the collision or scattering in the channel region of the pentacene layer. Therefore, the I_{DS} and field effect mobility of the FET (μ_{FET}) decreased, which can be explained by the equation[13]

$$\mu_{FET} = \frac{\upsilon_{dp}}{E} = \frac{\varepsilon\tau_{cp}}{m_p^*} \tag{3}$$

where υ_{dp} is the average drift velocity of the holes, E is the electric field, e is the magnitude of the electronic charge, τ_{cp} is a mean time between collisions or scattering and m^* is the effective mass of the hole. We expect the τ_{cp} to decrease depending on the increase of collision or scattering at the channel region due to attracted holes. This sensing mechanism of the GOSS based biosensor is illustrated in Fig. 1B.

We performed a concentration based study to obtain a relation between the concentration of DNA and the mobility reduction. Different concentrations of polyT ranging from 0.1 pmoles μL^{-1} to 100 pmoles μL^{-1} were injected on the GOSS-pentacene FET treated with polyA (10 pmoles μL^{-1}). The normalized mobility reduction in the FET with increasing polyT concentration is shown in Fig. 4F. Due to the increase in hybridization, the total amount of negative charge increased on the GOSS, thus resulting in higher mobility reduction. Based on the signal obtained from the blank, non-target DNA. The sensing limit was estimated to be 0.1 pmoles μL^{-1} of the GOSS-pentacene FET based sensor.

3.4 Detection of SkBr3 cells

To study the versatility of the GOSS in bio-sensing different biomolecules, we also detected the CTCs such as SkBr3 associated with breast cancer. The HER2 positive SkBr3 cells were detected using the GOSS-pentacene FET while MCF-7 cells were used as an HER2 negative cell. Herein, the GOSS ink was pretreated with the HER2 antibody. The HER2 receptor was characterized quantitatively and the expression level of HER2 in SkBr3 and MCF-7 cell lines was analyzed by western blot (Fig. S3, ESI†). The MCF-7 cell has an HER expression of 11.38 when the expression level of the SkBr3 cell is normalized to 100. Firstly, we confirmed the antigen–antibody interaction on the GOSS using a fluorescence microscope as shown in Fig. 5A. 2 μL (100 EA per μL) of each cell type was injected into the fluid channel of different devices. We used rhodamine B-isothiocyanate (RITC) and GelGreen staining to discriminate the GOSS and attached CTCs. The GOSS was pre-stained with RITC before printing and followed by GelGreen staining of the cells.

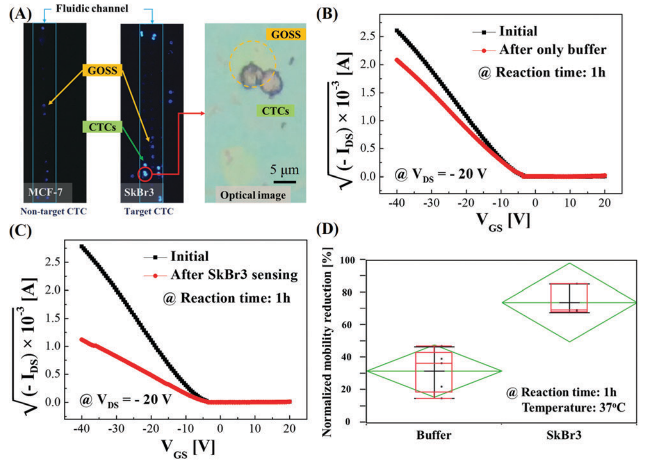

Fig. 5 (A) Fluorescence image of the GOSS surface with different cell lines: HER2 negative (non-target) MCF-7 cells (left) and HER2 positive (target) SkBr3 cells (right); the optical image of captured SkBr3 on GOSS. (B) Electrical performance of the GOSS-pentacene FET. The transfer curve (V_{DS} = −20 V) of the FET before and after buffer injection, and (C) after SkBr3 injection. (D) Change in the normalized mobility of the FET after buffer and SkBr3 cell injection (n = 3). The standard deviation values of the sensing result for buffer and SkBr3 are 0.12 and 0.09, respectively.

In Fig. 5A, the dark blue spots represent the GOSS while the lighter and brighter green spots represent the CTCs. When the MCF-7 cells were added on the FET, the staining of the surface did not produce any bright green spots, confirming the absence of an antigen–antibody interaction. Further, bright green spots appeared on the FET when SkBr3 cells were added, confirming the antigen–antibody interaction. The optical microscopic imaging as shown in Fig. 5A also validated the selective attachment of CTCs.

The detection of CTCs was initiated by injecting 2 μL (100 EA per μL) of SkBr3 cells on the antibody modified GOSS. The analysis was performed by measuring the difference in electrical properties of the blank (only buffer) and after CTC attachment. Fig. 5B and C shows the electrical performance of the two devices. In the case of blank, the ions present in buffer affected the FET, thereby reducing by 40% of the mobility. In the case of SkBr3 cells attachment, the mobility dramatically decreased by 95% of the mobility. Although the overall net charge of the cell membrane is neutral, the outermost hydrophilic head contains the negatively charged phosphate group and glycerol. This surface negative charge scatters the holes in the pentacene channel and affects the electrical performance.

Fig. 5D shows the comparison of three independent sensing results of buffer and SkBr3 cells. The average mobility reduction by the buffer is 3.231% with a standard deviation of 0.12. Meanwhile, for SkBr3 cells, the mean mobility reduction was 74.3% with a standard deviation of 0.09. Based on these results, we again confirm the versatility, high sensitivity, and reproducibility of the GOSS based pentacene FET biosensor.

Recently, techniques such as the fabrication of an additional floating gate, addition of nanoparticles, and deposition of a polymer layer on top of the organic semiconductor have been reported for attachment of capture sites.[14] Although these devices have been proven to be effective, just the physical attachment of the sensing and active layer prevents their direct interaction, resulting in decreased sensitivity. In contrast, the aromatic rings of pentacene and the GOSS form π–π bonding, thus enabling their direct interaction. To the best of our knowledge, this is the first time that the inkjet printed GOSS-pentacene FET (functionalized GO ink) based biosensor has been reported.

The GO has still a negative charge after amination but not much than before. Also, the biomolecules with negative charge generally is difficult for binding with only aminated GO. But the partially positive charge region owing to the primary amine onto the GO could be weakly introduced for non-specific binding with the biomolecules. Therefore, we modified the GO composite with the DNA strand or cancer antibody for increasing specific binding to the target DNA or cancer cell. The GOSS based biosensor showed good performance in detecting DNA and SkBr3 cells.

The GO can be easily functionalized in bulk for the label-free detection of target analytes. Furthermore, the GOSS can be synthesized independently and integrated with different sensors, without exposing the actual sensor to different chemicals.

4 Conclusion

We successfully synthesized the GOSS and demonstrated a GOSS-pentacene FET for the specific bio-sensing of DNA and CTCs. The GOSS was inkjet printed on the pentacene and provided binding sites for the analytes. The mobility of the FET biosensor significantly changed due to the negative charge of the captured target DNAs and CTCs. The FET showed very sensitive performance with a detection limit of 0.1 pmoles for DNA and 100 cancer cells per detection volume (μL). From these results, the GOSS-pentacene FET proved to be highly stable and reproducible. Moreover, the GOSS can be easily synthesized in bulk and independently to obtain a sensing layer of choice. Our approach will be valuable for a prospective, flexible, low-cost and label-free multiplex diagnostic platform. In the future research, this multiplex GOSS-pentacene biosensor will be combined with integrated circuits to demonstrate a wireless point-of-care sensor.

Acknowledgements

T. Yoon was supported by the GRRC program of Gyeonggi province (GRRC 2016B02, Photonics-Medical Convergence Technology Research Center).

References

1 S. Cheng, S. Hideshima, S. Kuroiwa, T. Nakanishi and T. Osaka, *Sens. Actuators, B*, 2015, **212**, 329–334.
2 J. M. Park, M. S. Kim, H. S. Moon, C. E. Yoo, D. Park, Y. J. Kim, K. Y. Han, J. Y. Lee, J. H. Oh, S. S. Kim, W. Y. Park, W. Y. Lee and N. Huh, *Anal. Chem.*, 2014, **86**, 3735–3742.
3 S. Shah, J. Smith, J. Stowell and J. Blain Christen, *Sens. Actuators, B*, 2015, **210**, 197–203.
4 K. A. Hyun, T. Y. Lee, S. H. Lee and H. I. Jung, *Biosens. Bioelectron.*, 2015, **67**, 86–92.
5 N. M. Karabacak, P. S. Spuhler, F. Fachin, E. J. Lim, V. Pai, E. Ozkumur, J. M. Martel, N. Kojic, K. Smith, P.-i. Chen, J. Yang, H. Hwang, B. Morgan, J. Trautwein, T. a. Barber, S. L. Stott, S. Maheswaran, R. Kapur, D. a. Haber and M. Toner, *Nat. Protoc.*, 2014, **9**, 694–710.
6 S. W. Lee, K. A. Hyun, S. I. Kim, J. Y. Kang and H. I. Jung, *J. Chromatogr. A*, 2015, **1377**, 100–105.
7 S. Jeon, J.-M. Moon, E. S. Lee, Y. H. Kim and Y. Cho, *Angew. Chem., Int. Ed.*, 2014, **53**, 4597–4602.
8 S. Sang, Y. Wang, Q. Feng, Y. Wei, J. Ji and W. Zhang, *Crit. Rev. Biotechnol.*, 2015, **36**, 1–17.
9 N. Gao, W. Zhou, X. Jiang, G. Hong, T.-M. Fu and C. M. Lieber, *Nano Lett.*, 2015, **15**, 2143–2148.
10 N. S. Green and M. L. Norton, *Anal. Chim. Acta*, 2015, **853**, 127–142.
11 X. Strakosas and M. Bongo, *J. Appl. Polym. Sci.*, 2015, **132**, 1–14.
12 H. Yang, C. Yang, S. H. Kim, M. Jang and C. E. Park, *ACS Appl. Mater. Interfaces*, 2010, **2**, 391–396.
13 J.-m. Kim, S. Kumar, R. Chand, D.-h. Lee and Y.-s. Kim, *Biosens. Bioelectron.*, 2011, **26**, 2264–2269.
14 M. H. Park, D. Han, R. Chand, D. H. Lee and Y. S. Kim, *J. Phys. Chem. C*, 2016, **120**, 4854–4859.
15 B. Veigas, E. Fortunato and P. V. Baptista, *Sensors*, 2015, **15**, 10380–10398.
16 H. U. Khan, M. E. Roberts, W. Knoll and Z. Bao, *Chem. Mater.*, 2011, **23**, 1946–1953.
17 H.-C. Chen, Y.-T. Chen, R.-Y. Tsai, M.-C. Chen, S.-L. Chen, M.-C. Xiao, C.-L. Chen and M.-Y. Hua, *Biosens. Bioelectron.*, 2015, **66**, 198–207.
18 L. Gonzalez-Macia, A. Morrin, M. R. Smyth and A. J. Killard, *Analyst*, 2010, **135**, 845–867.
19 N. Komuro, S. Takaki, K. Suzuki and D. Citterio, *Anal. Bioanal. Chem.*, 2013, **405**, 5785–5805.
20 A. Määttänen, U. Vanamo, P. Ihalainen, P. Pulkkinen, H. Tenhu, J. Bobacka and J. Peltonen, *Sens. Actuators, B*, 2013, **177**, 153–162.
21 T. Wang, C. Cook and B. Derby, *Proceedings – 3rd International Conference on Sensor Technologies and Applications*, 2009, pp. 82–85.
22 A. Bietsch, M. Hegner, H. P. Lang and C. Gerber, *Langmuir*, 2004, **20**, 5119–5122.
23 M. Carbone, L. Gorton and R. Antiochia, *Electroanalysis*, 2015, **27**, 16–31.
24 T. Kajisa and T. Sakata, *Jpn. J. Appl. Phys.*, 2015, **54**, 04DL06.
25 F. A. Sarbani Basu and Y.-H. Wang, *Nanotechnology*, 2014, **25**, 085201.